JOURNAL OF Applied Polymer SCIENCE

Nucleation Parameter and Size Distribution of Critical Nuclei for Nonisothermal Polymer Crystallization: The Influence of the Cooling Rate and Filler

Nikola Kocic, Sara Lederhofer, Karsten Kretschmer, Martin Bastian, Peter Heidemeyer
SKZ – German Plastics Center, Wuerzburg, Germany
Correspondence to: N. Kocic (E-mail: n.kocic@skz.de)

ABSTRACT: The nucleation parameter K_g of filled PP, HDPE, and PA6 is determined through nonisothermal DSC measurements. A novel method is proposed for the determination of the size distribution of critical nuclei, where the most commonly found fraction l^*_{peak} was obtained as a peak value. The models are tested at different cooling rates and different filler loadings. K_g varies up to a certain cooling rate and afterwards remains constant. The introduction of talc in PP and HDPE facilitates nucleation and thus reduces K_g. An opposite trend occurs upon the addition of bentonite in PA6. The changes of K_g and l^*_{peak} are reflected on sample morphology, as confirmed with SAXS. The ratio between the final crystal thickness and l^*_{peak} amounts to approx. 2 and thus agrees well with the one listed in literature. The simple linear correlations of the obtained K_g are established with Young's modulus and yield stress.
 J. Appl. Polym. Sci. **2015**, *132*, 41433.

KEYWORDS: composites; crystallization; morphology; theory and modeling; thermoplastics

Received 27 May 2014; accepted 21 August 2014
DOI: 10.1002/app.41433

INTRODUCTION

The nuclei formation during the polymer crystallization is governed by the lowering of the Gibbs free energy associated with the formation of the more stable crystalline phase, but destabilized by the increase in free energy associated with the creation of a new solid surface.[1,2] As a result, Gibbs free energy shows a maximum ΔGn*, which can be regarded as being the activation energy barrier, which needs to be overcome to form a stable nucleus, which will grow further.[3] Assuming that nucleation occurs on a preexisting substrate (secondary nucleation) and a critical nucleus of rectangular shape with the thickness l^* much smaller compared to the other two dimensions. Thus, the activation energy barrier ΔGn* and the critical nuclei thickness l^*_c at a given temperature T can be written down in the following form:[4,5]

$$\Delta G^*_n \sim \frac{K_g}{\Delta T} \tag{1}$$

$$l^*_c = \frac{2\sigma_e T^0_m}{\Delta H^\theta_f \left(T^0_m - T\right)} \tag{2}$$

where K_g is the nucleation parameter, which can be regarded as being the energy required for the formation of a secondary nucleus of a critical size, σ_e is the fold surface free energy, which measures the work required to create the face surface of the crystal nuclei, ΔH^θ_f is the change in enthalpy per unit volume, that is, the heat of fusion per unit volume of an ideal crystal and $T^0_m - T$ is the supercooling (ΔT), whereby T^0_m denotes the equilibrium melting temperature. To enter the thermodynamically stable state, the nuclei have to overcome critical thickness $l_c{}^\star$ defined with eq. (2):[6]

$$l_i = l^*_c + \delta l \tag{3}$$

where δl is the thickness increment, which enables the critical nucleus to enter the thermodynamically stable state at the fastest rate:[4]

$$\delta l = \frac{k_b T_{peak}}{2 b_0 \sigma} \left(\frac{4\sigma + a_0 \Delta H^\theta_f}{2\sigma + a_0 \Delta H^\theta_f} \right) \tag{4}$$

where σ is the side surface free energy, a_0 and b_0 are the width and thickness of the chain stem, k_b being the Boltzmann constant. The subcritical nuclei with a thickness $<l_c{}^\star$ dissolve back into the liquid phase. Thus, the thickness of the fastest growing, thermodynamically stable nuclei (l_i) can be regarded as being the initial crystal thickness. Further crystal thickening above l_i can occur, depending upon the structure and segmental mobility of the macromolecules[6] to give the final crystal thickness (l_c):[7]

$$l_c = \gamma_{HW} \left(l^*_c + \delta l \right) \tag{5}$$

γ_{HW} being the Hoffman-Weeks thickening coefficient.

The nucleation parameter K_g in eq. (1) is assumed to be temperature-independent. It is defined as follows:[8]

$$K_g = \frac{\xi b_0 \sigma \sigma_e T_m^0}{k_b \Delta H_f^\theta} \tag{6}$$

In eq. (6) the parameter ξ is a regime-dependent constant. By knowing K_g, one can easily calculate the fold surface free energy σ_e, which in turn can be used to determine the thickness of the critical nucleus l_c^*, which is related to the final crystal thickness. Hence, K_g could be a link to connect the crystallization process and morphology of semicrystalline polymers.

The Hoffman growth-rate equation in double logarithmic transformation is generally used to obtain the nucleation parameter K_g analysing the isothermal crystallization of polymer materials at a temperature T_c:[9,10]

$$\ln(G(T)) + \frac{U}{R(T - T_\infty)} = \ln(G_0) - \frac{K_g}{T\Delta T} \tag{7}$$

In eq. (7), $G(T)$ denotes the crystal growth rate, G_0 denotes the pre-exponential factor, which accounts for the factors that affect the transport of macromolecular chains toward the growing site, U is the activation energy for the transport of polymer segments to the site of crystallization, T_∞ is the theoretical temperature at which all motion associated with viscous flow or reptation ceases and is defined as $T_\infty = T_g - 30$, T_g is the glass transition temperature and R is the universal gas constant. The values of G_0 and U are temperature-independent. If the left side of eq. (7) is plotted against $1/(T\Delta T)$, a straight line with the K_g as a slope should be obtained, when the model adequately represents the process. The critical break points that appear in such a plot, identified by the change in the slope of the line by factor 2, have been attributed to regime transitions. If the rate of nucleus formation is much lower than the nucleus spreading rate, regime I occurs and parameter ξ in eq. (6) is equal to 4. Regime II occurs when the two rates are comparable ($\xi = 2$) and regime III when the rate of nucleation is greater than the rate of spreading ($\xi = 4$).[11] Hence, K_g in regime I is equal to K_g in regime III, while K_g in regime II is half of that in regime I and III. Regarding isothermal crystallization, the crystal growth rate G in μm/s necessary to fit eq. (7) is usually determined experimentally using hot-stage microscopy.[12] However, eq. (7) cannot be used in combination with thermal analysis like DSC, which measures the overall crystallization rate instead of the crystal growth rate. Another practical limitation of eq. (7) is that it is applicable only in case of isothermal crystallization. The isothermal measurements are, however, often restricted to a narrow crystallization temperature range, since the response time of the measuring system must be small, compared to the overall crystallization time. The actual processing is also often nonisothermal in nature. Hence, examinations under nonisothermal conditions are a useful complement to understand the crystallization of polymers during the process. So far there have been few attempts to adapt eq. (7) to nonisothermal DSC measurements, which is a conveniently accessible, simple and fast experimental technique.[13–17] However, the proposed models are either applicable only with more than one DSC-measurement performed under different cooling rates,[14,15] or in a narrow temperature region.[15] Additionally, the Monasse-Haudin model[17] which is applied to find the K_g of pure PP, does not give satisfactory results concerning filled semicrystalline polymers, such as talc-filled PP, as shown in Kocic et al.[18] The reason could be the strong nucleating effect of talc, which changes the way of nucleation and growth of PP crystals.

In our last publication, we tried to adapt the Monasse-Haudin model[17] to the filled polymers. The following equation was obtained:[18]

$$\ln\left(\frac{d(\ln(1-X(T)))}{\mathrm{dT}}\right) - \frac{m}{m+1}\ln(-\ln(1-X(T)T)) + \frac{U}{R(T-T_\infty)} = (\ln(G_0)+\phi) - \frac{K_g}{T\left(T_m^0 - T\right)} \tag{8}$$

In eq. (8), ϕ is a constant and $X(T)$ is the relative degree of crystallinity as a function of temperature. It is defined as the degree of transformation from the melt amorphous to the solid, partly crystalline state and thus takes the values between 0 and 1. $X(T)$ can be calculated from the nonisothermal DSC measurements as the ratio between the measured enthalpy of crystallization released from the beginning of crystallization up to temperature T and the total enthalpy released during the whole crystallization process:

$$X(T) = \frac{\int_{T_{\mathrm{onset}}}^{T} \frac{dH}{dT}\, dT}{\int_{T_{\mathrm{onset}}}^{T_{\mathrm{end}}} \frac{dH}{dT}\, dT} \tag{9}$$

where dH denotes the measured enthalpy of crystallization during an infinitesimal temperature interval dT. The limits T_{onset} and T_{end} are used to denote the onset and end crystallization temperatures, respectively.

The best linear correlation of eq. (8), which is necessary to calculate the K_g as a slope was obtained by defining the fit parameter m as $n-2$, whereby n was determined as a slope by fitting $X(t)$ and t obtained from nonisothermal DSC measurements into the double logarithmic form of the Avrami equation,[19] which was used here only as a fit function:

$$\log(-\ln(1-X(t))) = \log(K) + n\log(t) \tag{10}$$

Using the proposed mathematical procedure and nonisothermal DSC measurements under a cooling rate of 10 K/min, the nucleation parameter K_g of talc-filled PP was obtained. It was observed that the calculated K_g decreases with the decreased talc particle sizes d_{50} as a consequence of the increased nucleation ability of the talc having smaller particles. For the composite with 5 wt % of talc; however, no dependence of K_g on d_{50} was observed. It was assumed that for such a low talc concentration, the cooling rate of 10 K/min is too low, so that the homogeneous nucleation prevails compared to talc-induced heterogeneous nucleation. Thus, to confirm this assumption, further DSC studies of composites with a lower amount of talc (between 0 and 5 wt %) under a cooling rate >10 K/min are needed.

This work constitutes a continuation of our previous study. In the first section, the novel approach is presented that allows one

Table I. The Main Properties of the Talc Used (Manufacturer Data)

Talc type	d_{50} (μm)	d_{98} (μm)	Specific surface BET (m^2/g)
Fintalc M03	1.0	6.0	13.0
Fintalc M10	2.8	13.0	8.0
Fintalc M30	10.0	27.0	3.5

to determine the size distribution of the critical nuclei (l_c^*) during the nonisothermal DSC-scan. The influence of the cooling rate and filler content on the nucleation parameter (K_g) and size distribution of the critical nuclei is investigated in the second and third section, respectively. In the last section, the correlations of the obtained K_g with mechanical properties (Young's modulus and yield stress) are established and discussed.

EXPERIMENTAL

Materials

Polypropylene (PP) HD120MO, which is 95% isotactic, with a weight-average molecular weight $M_w = 365$ kg/mol, polydispersity $M_w/M_n = 5.4$ and melt flow index (MFI) = 8 g/10 min at 230°C/2.16 kg was kindly supplied from Borealis. This grade of PP is not nucleated, does not contain antistatic agents, contains an antioxidant package based on phosphites/phenolics and a stearate-based acid scavenger. The pure HDPE B6246LS used in this study was provided by from Sabic. It has a M_w of 115 kg/mol, M_w/M_n of 7.6 and MFI of 0.5 g/10 min at 190°C/2.16 kg. For our study pure polyamide 6 (PA6), type Ultramid B36 01 was provided by BASF, with a M_w of 26 kg/mol, M_w/M_n of 3.8 and relative viscosity of 3.6 (1% in 96% sulphuric acid).

Three talc grades of the same origin and with different particle sizes were supplied by Mondo Minerals. Fintalc M10 and M30 were used as ingredients in PP, while Fintalc M03 was used in HDPE. The main properties of the talc types used in this study are summarized in Table I.

Organically modified, nanodispersible layered silicate under the trade name Nanofil SE 3010 (LOI 43%, moisture content < 3%), was provided by Byk Additives and used as an ingredient in PA6. It was produced by treating a natural bentonite with a dimethyl, di(hydrogenated tallow)alkyl ammonium salt. The layer spacing (d-spacing) of Nanofil SE 3010 determined in this work with small angle X-ray scattering (SAXS) amounts to 33 Å.

Sample Preparation

The PP compounds with 0, 0.1, 0.2, 0.3, 0.4, 0.5, and 1.5 wt % of talc M10 and M30 were prepared by melt mixing on a Leistritz (model ZSE27Maxx) corotating twin-screw extruder ($L = 1188$ mm and $D = 27$ mm), with a temperature profile from 225 down to 205°C (die), a screw speed of 280 min^{-1} and a throughput of 40 kg/h. After compounding, the pellets were air dried at 80°C for 1 h in a drying chamber and injection molded using the Battenfeld HM 150/350 machine, with barrel temperatures of 200, 210, 220, and 220°C (die), a mold temperature of 25°C, an injection rate of 70 cm^3/s, and a holding pressure of 800 bar.

The films, 2.8 mm thick and 300 mm wide, made of pure HDPE as well as of HDPE with 1.0, 1.5, 2.0, and 3.0 wt % of Fintalc M03, were prepared in a direct film extrusion process, using the same twin screw extruder as for the PP compounds. In this process, the forming tool is connected directly to the extruder. Accordingly, this method combines mixing and shaping, enabling the production of semi-finished products such as films, plates, tubes, or profiles in a single process step. The temperature profile of the extruder ranged from 175 to 205°C (die). The throughput and screw speed were 15 kg/h and 600 min^{-1}, respectively.

PA6/nanoclay compounds were prepared using the same twin screw extruder as for the PP/talc and HDPE/talc compounds, with barrel temperatures between 145 and 250°C, a throughput of 30 kg/h and a screw speed of 600 min^{-1}. After compounding, the pellets were air dried at 80°C for 6 h and compression molded at 250°C under the pressure of 80 bar and a cooling rate of 15 K/min using a P300P press from Dr. Collin.

To check if the proposed filler concentrations were reached, an annealing of the compounded granulate was performed according to DIN EN ISO 3451-1 at 600°C for 3 h. The results of the annealing are listed in Table II. For the graphical presentation of the results in this work, the "reached" filler contents are applied. In the corresponding explanations, however, for the sake of clarity, the "desired" filler contents were used.

Sample Characterization

Non-isothermal DSC measurements were performed in accordance to DIN EN ISO 11357 using a nitrogen atmosphere in a Netzsch 204 F1 Phoenix differential scanning calorimeter. Indium, zinc, lead, bismuth, and tin standards were used for temperature calibration. Depending on the material of interest, the measurements were performed following different programs. As regards PP/talc, the samples of 18.4 ± 0.5 mg were first heated from room temperature to 205°C with the rate of 10 K/min, held for 5 min at this temperature to erase the former thermal history, and subsequently cooled at a defined rate in the range between 10 and 30 K/min to room temperature.

Table II. A Comparison of the Desired and Obtained Talc Concentration After Annealing at 600°C for 3.5 h

Filler content "desired" (wt %)	Filler content "reached" (wt %)			
	Fintalc M10 in PP	Fintalc M30 in PP	Fintalc M03 in HDPE	Bentonite in PA6
0.10	0.13	0.16	-	
0.20	0.21	0.23	-	
0.30	0.33	0.34	-	
0.40	0.44	0.42	-	
0.50	0.52	0.50	-	0.53
1.00	-	-	1.00	1.07
1.50	1.50	1.49	1.55	1.68
2.00	-	-	1.97	2.18
3.00	-	-	3.07	3.27

Regarding HDPE/talc, the samples of 10 ± 0.1 mg were heated from room temperature to 220°C at a rate of 10 K/min. Subsequently, the samples were held at 205°C for 5 min and afterwards cooled at a defined rate to room temperature. Nonisothermal DSC-measurements of PA6/nanoclay were performed by heating the samples of 10 ± 0.1 mg to 280°C with a rate of 10 K/min and holding this temperature for 5 min. The samples were subsequently cooled at a defined rate to room temperature. For the modeling, the data obtained from the first DSC cooling cycle was used. Three DSC measurements were performed for each sample and all the subsequent calculated values are averages obtained from the three measurements.

For the characterization of the crystal structure, wide-angle X-ray scattering (WAXS) was performed. The data were recorded using a D8 Discover diffractometer from Bruker. The CuKα radiation source was operated at 40 kV and a current of 120 mA. A 2θ scan was performed at a scan speed of 0.3°/min in the 2θ range from 5 to 50°.

The crystalline long period (D), crystal thickness (l_c), crystallinity (X_{SAXS}), crystal orientation factor (ω) as well as the interlayer distance of the bentonite clay particles (d) were determined using a NanoStar small-angle X-ray scattering (SAXS) with a 2-D detector and CuKα radiation (45 kV/650 μA). The sample-detector distance was 106.5 cm and the measurements were conducted in the transmission mode in the 2θ range from 0.01 to 5°.

Young's modulus and yield stress were measured on a Zwick Z010 universal tensile test machine at 22,5°C and 53% relative humidity according to ISO 527-1, −2, and −3. The cross-head speed was 1 mm/min regarding Young's modulus and 50 mm/min regarding yield stress. At least five samples were tested for each material composition and the average value is reported.

RESULTS AND DISCUSSION

The Relative Size Distribution of the Critical Nuclei: Model Development

In this research, three different materials are used: PP filled with talc, high-density polyethylene (HDPE) filled with talc and PA6 filled with bentonite. In these three materials, the filler has a strong positive, a weak (positive) and a negative influence on the nucleation of a given polymer, respectively. To avoid mechanical reinforcement, the filler amount was kept low. All crystallographic, thermodynamic and nucleation constants used for the calculations in this work are listed in Table AI of the Appendix.

The change of the critical nuclei thickness (l_c^*) upon the infinitesimal change of temperature (dT) during DSC cooling can be obtained using a similar procedure to the one suggested by Alberola et al.[20] In contrast to Alberola, who used the Gibbs-Thomson equation as a starting point to find the final crystal thickness from the DSC heating step, we start from the Hoffmann equation for secondary nucleation [see eq. (2)]. Accordingly, the change of the critical nuclei thickness (l_c^*) with the infinitesimal temperature change (dT) during a cooling step can be defined as follows:

$$\frac{dl_c^*}{dT} = \frac{2\sigma_e T_m^0}{\Delta H_f^\theta \left(T_m^0 - T\right)^2} \tag{11}$$

and the change of the relative degree of crystallinity defined by eq. (9) as:

$$\frac{dX}{dT} = \frac{\frac{dH}{dT}}{\Delta H_f} \tag{12}$$

whereby dH/dT (in J/gK) denotes the energy released between T and $T - dT$ and corresponds to the DSC signal at this point and ΔH_f is the total amount of energy released during the whole DSC cooling. Now, the distribution of the critical nuclei thickness can be defined as follows:

$$\text{distribution} = \frac{1}{X_{\text{end}}}\frac{dX}{dl^*} = \frac{dX}{dl^*} \tag{13}$$

where X_{end} in eq. (13) denotes the relative degree of crystallinity at the end of the crystallization process and thus takes the value of 1.

Through the combination of eqs. (11), (12), and (13), the distribution of the initial crystal thickness during the DSC cooling step can be calculated as follows:

$$\text{distribution} = \frac{\left(T_m^0 - T\right)^2 \frac{dH}{dT} \Delta H_f^\theta}{2\Delta H_f \sigma_e T_m^0} \tag{14}$$

In eq. (14) the fold surface free energy σ_e can be obtained from eq. (6), whereby the nucleation parameter K_g can be calculated using the method proposed in our previous publication [see eq. (8)].

The Influence of the Cooling Rate at a Constant Filler Amount

In this section, the filler content was kept constant and amounted to 0.5 wt % of Fintalc M10 and M30 in PP, 2 wt % of Fintalc M03 in HDPE and 2 wt % of bentonite in PA6. The examples of the DSC exotherms obtained by varying the cooling rate are plotted in Figure 1. As can be seen, the exothermic peak becomes wider and shifts toward lower temperatures with an increased cooling rate. This phenomenon is already known for many polymers and is true for all of the samples studied in this work. The shift of the crystallization curves is a consequence of the inequality between the incubation period, defined as the time required before the critical nucleus dimension is established[21] and the residence time that the sample spends at each temperature during a nonisothermal scan. The incubation time is a direct function of critical nuclei thickness: the thicker the critical nucleus, the more time is needed for its formation, that is, the incubation period is longer. The thickness of the critical nucleus is, according to eq. (2), a function of temperature: higher temperatures in DSC scans correspond to thicker critical nuclei and thus to a longer incubation time. However, by increasing the cooling rate, the residence time is reduced and is much lower in the high temperature region compared with the incubation time. Accordingly, the critical nuclei cannot be established. Nevertheless, the polymer itself responds by shifting the crystallization process toward lower temperatures, that is, toward the thinner critical nuclei and thus lowering the incubation time.

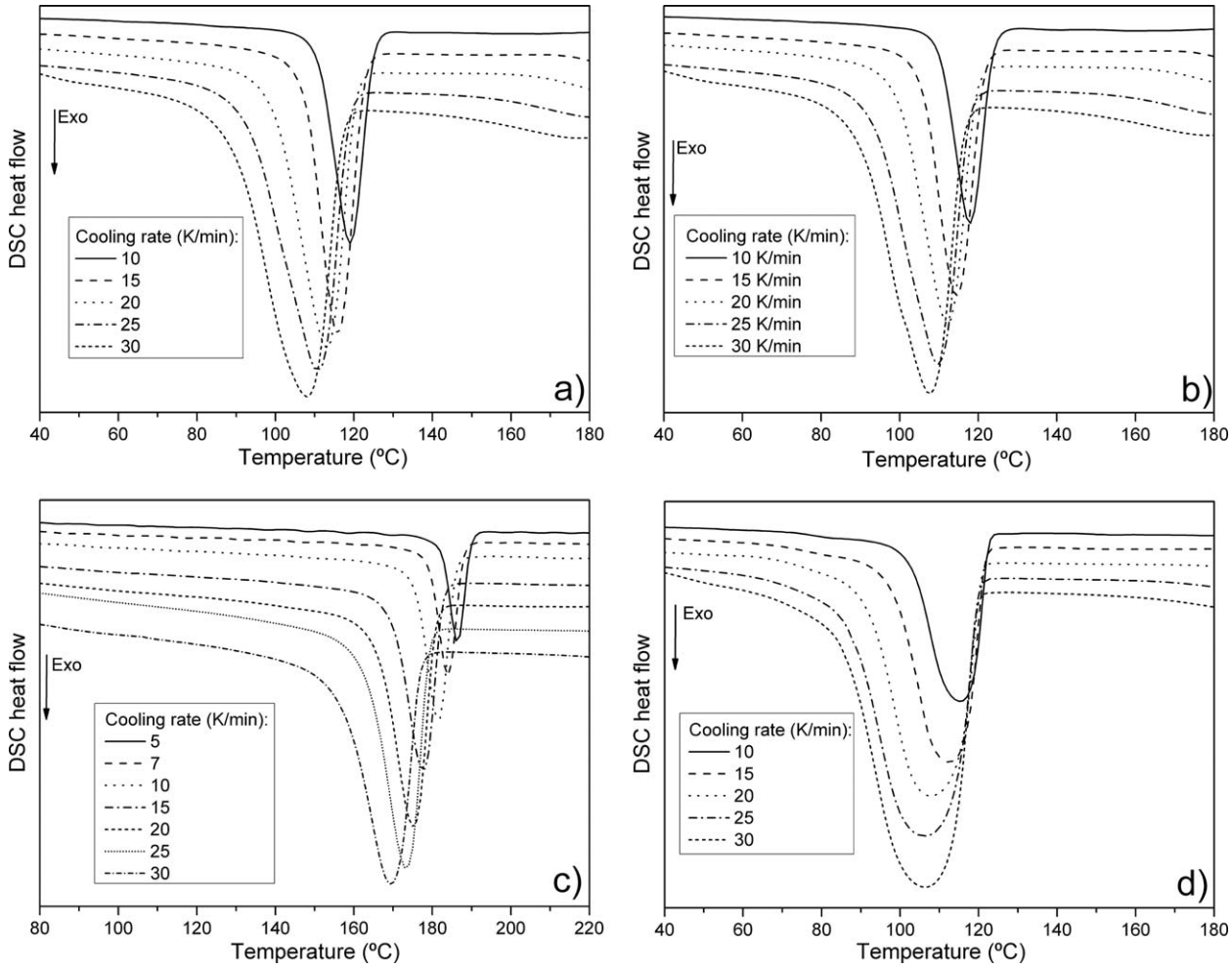

Figure 1. Nonisothermal DSC exotherms at various cooling rates for: (a) PP with 0.5 wt % of Fintalc M10; (b) PP with 0.5 wt % of Fintalc M30; (c) PA6 with 2 wt % of bentonite; (d) HDPE with 2 wt % of Fintalc M03.

As shown in our previous publication,[18] eq. (8) gives a satisfactory agreement with experiments in the range of relative crystallinity $[X(T)]$ between ~0.035 and 0.98. Therefore, the relative crystallinity $[X(T)]$ in the range between ~0.035 and 0.98 was calculated from the exotherms presented in Figure 1 according to eq. (9) and afterwards used to fit eq. (8). The results of linear fitting for three materials at different cooling rates are presented in Figure 2. As can be seen, eq. (8) gives a satisfactory agreement with the experiments. The correlation coefficient R^2 was not <0.984 in all cases. As a consequence of the reduced residence time with an increased cooling rate, the lines are shifted in the direction of the lower temperatures. Furthermore, regarding PP and HDPE samples, a deviation from the ideal linearity increases (R^2 decreases) with an increased cooling rate. However, for PA6 sample no deterioration of the ideal correlation with an increased cooling rate is observed. The deviation from the ideal linearity obtained in Figure 2 can be a consequence of the non-isothermal effects described well by Sajkiewicz.[22]

For a polymer crystallizing at a constant temperature (isothermal crystallization), its overall crystallization rate is a function of temperature. Nevertheless, when it comes to nonisothermal crystallization it is believed that there are two nonisothermal effects: transient and athermal effects. The consequence of both effects is a dependence of the crystallization rate on the rate of temperature change.

According to eq. (8), the nonisothermal DSC scan is approximated with a finite number of isothermal segments. Accordingly, the crystallization rate depends only on the instantaneous temperature in every single segment of the DSC scan and is independent of the rate of temperature change. Thus, at each DSC temperature, the steady-state value of the crystallization rate is assumed to be reached immediately. Nevertheless, when a polymer is transferred to a new condition by lowering the temperature during the cooling, the achievement of a steady-state rate defined by the current temperature does not occur instantaneously, but rather some time is needed to "switch" the crystallization rate between the previous and the current conditions. As a consequence, the current crystallization rate deviates from that defined by the current temperature.[23] This is the so-called transient or relaxational effect.[24] The transient effect causes the lag of crystallization behind the changes of external conditions. In the upper branch of the nonisothermal DSC plot presented in Figure 1, up to the crystallization peak temperature, the

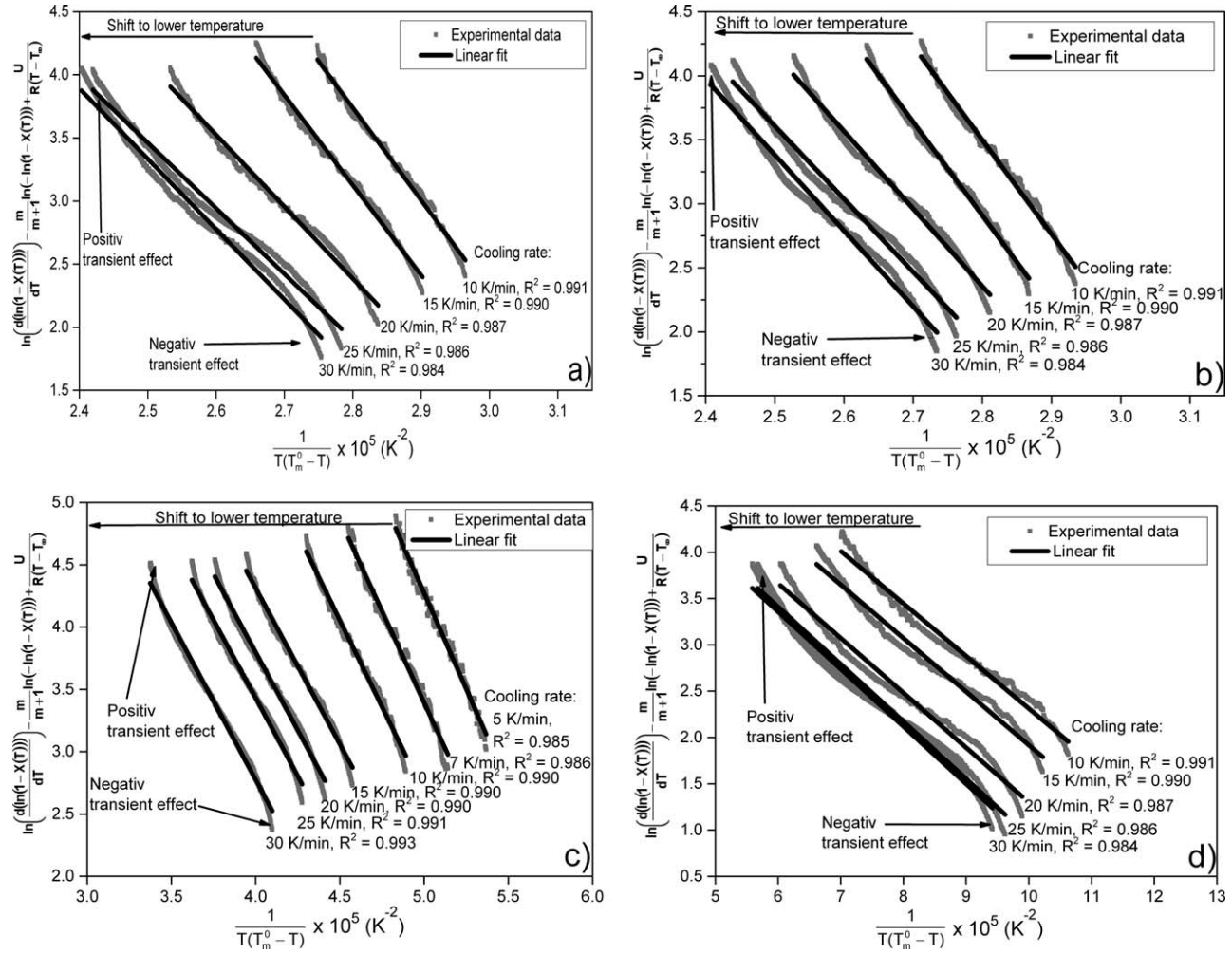

Figure 2. The fitting of the experimental data [X(T) and T)] with eq. (8) at different cooling rates for: (a) PP with 0.5 wt % of Fintalc M10; (b) PP with 0.5 wt % of Fintalc M30; (c) PA6 with 2 wt % of bentonite; (d) HDPE with 2 wt % of Fintalc M03.

temperature decrease leads to the increase of the crystallization rate. Therefore, in the upper part of the DSC plot, the negative transient effect slows down the crystallization rate. As a result, there is a decrease of relative crystallinity [X (T)] compared with the steady-state value defined at this temperature, which leads to the deviation of the ordinate value from ideal linearity in the lower part of the lines presented in Figure 2. However, the positive transient effect increases the crystallization rate in the lower part of the DSC plot shown in Figure 1, thus leading to the ordinate deviation in the upper part of the lines presented in Figure 2. As can be seen, the positive and negative transient effects cause the increase of the slopes of the linear correlations in Figure 2 and thus should lead to an increase of the nucleation parameter K_g. The deviation from the ideal linearity and thus the transient effect seems to be most pronounced with the HDPE sample shown in Figure 2(d). As opposed to this, the PA6 sample shows almost no deviation from the ideal linearity, as can be seen in Figure 2(c).

The second nonisothermal, so-called athermal effect, is proportional to the cooling rate.[23] To become stable, the nuclei have to achieve the critical thickness, which according to eq. (2) decreases when lowering the temperature. If the cooling rate is relatively high, the thin subcritical nuclei that were unstable under the initial condition will not dissolve, but will stay in the system and achieve the critical value at some lower temperature.[23] Accordingly, the athermal effect is believed to accelerate the crystallization rate in the whole temperature range by stabilizing the subcritical nuclei, which would otherwise be dissolved. Since their thickness is lower than the critical value, the stabilization of the subcritical nuclei should be reflected through the K_g reduction. The K_g values for the PP, HDPE, and PA6 samples were determined as the corresponding slopes in Figure 2 and in a function of the cooling rate presented in Figure 3.

As can be seen in Figure 3(a), the difference in the obtained K_g values of PP filled with 0,5 wt % of Fintalc M10 and M30 is visible only for the cooling rates $>\sim$20 K/min. We believe that up to $\sim$20 K/min, the thermal (homogeneous) nucleation occurred simultaneously to the heterogeneous, talc-induced nucleation. Accordingly, no clear difference between the nucleation effects of the two talc types with different particle sizes can be observed. For the higher cooling rates, however, the residual time that the sample spends at each temperature is too short

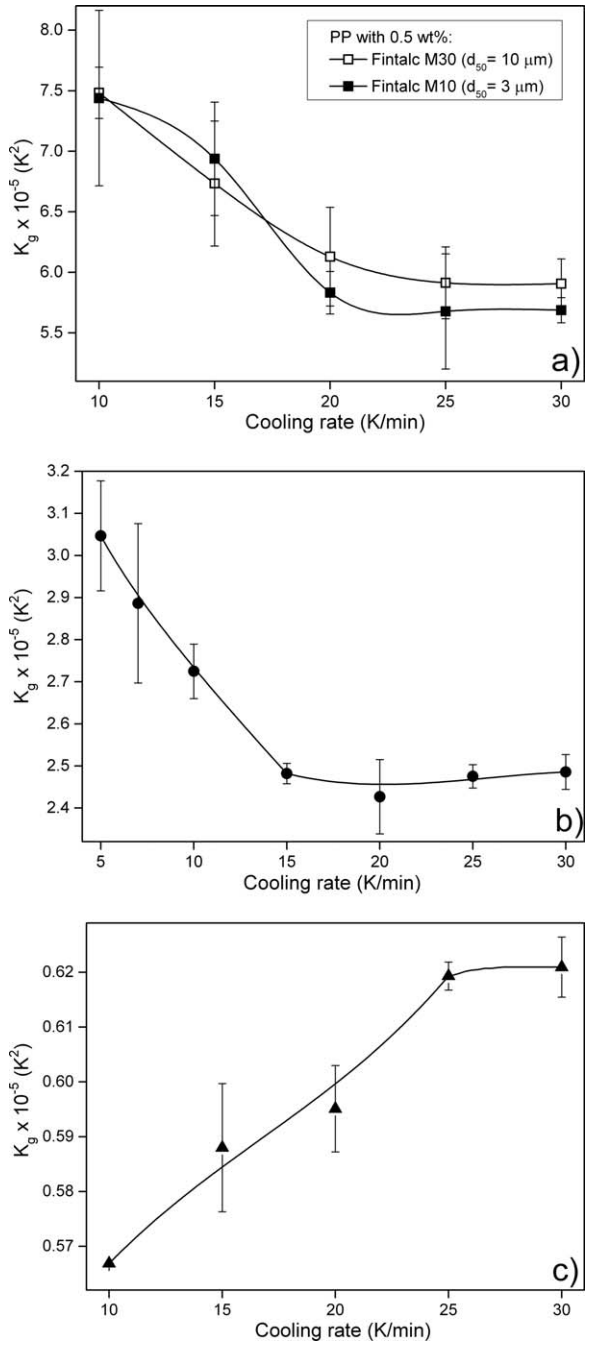

Figure 3. The obtained K_g values with respect to the cooling rate for: (a) PP with 0.5 wt % of Fintalc M10 and M30; (b) PA6 with 2 wt % of bentonite; (c) HDPE with 2 wt % of Fintalc M03.

for the formation of homogeneous nuclei. Thus, most nuclei that are formed at higher cooling rates are these, which can be formed faster, that is, heterogeneous nuclei. Accordingly, the corresponding K_g value depends on the talc type used to induce the heterogeneous nucleation. Fintalc M10 has smaller particles compared to Fintalc M30 and thus a higher specific surface, which means more area for the formation of the heterogeneous PP nuclei. This leads to a lower surface free energy (σ_e) and accordingly to eq. (6) a lower K_g of PP with Fintalc M10 for the cooling rates >20 K/min [see Figure 3(a)].

Furthermore, as can be clearly seen in Figure 3, opposite trends of K_g dependence are obtained. Considering the PP and PA6 samples [Figure 3(a,b)], K_g decreases up to a certain cooling rate (20 K/min for the PP samples i.e., 15 K/min for the PA6 sample) and afterwards shows a plateau up to 30 K/min. The decrease of K_g is a consequence of the pronounced athermal effect, which can stabilize the nuclei of PP and PA6. As opposed to PP and PA6, the K_g of the HDPE sample increases with the cooling rate up to 25 K/min [see Figure 3(c)] and afterwards remains unchanged. Compared with PP and PA6, HDPE possess a shorter repeating unit and no substituents in its chain structure. This leads to a low energy barrier of nucleation, which can be easily overcome. Therefore, only (or mostly) stable, that is, supercritical nuclei are formed during the nonisothermal crystallization of HDPE. Since the athermal effect acts on subcritical nuclei, the absence of subcritical nuclei of HDPE leads to the absence of an athermal effect. Thus, there remains only the transient effect, which promotes an increase in the nucleation parameter K_g of HDPE, as shown in Figure 3(c).

Furthermore, the size distribution of the critical nuclei during the nonisothermal cooling under different rates was determined using the proposed eq. (14). The fold surface free energy (σ_e) necessary for eq. (14) was obtained from the previously determined K_g and eq. (6). For this calculation, the K_g plateau value determined by the cooling rate of 30 K/min for PP- and HDPE-, that is, 15 K/min for the PA6-sample was applied. Additionally, to apply eq. (6), the parameter ξ and therefore the crystallization regime had to be determined. For this, the Lauritzen Z-test was used:[25]

$$Z = 10^3 \left(\frac{l_c}{2a_0}\right) \exp\left(-\frac{\varphi}{T_c \Delta T}\right) \tag{15}$$

where l_c is the crystal thickness and a_0 is the width of the chain stem (see Appendix). According to this test, regime I occurs if the substitution of $\varphi = K_g$ into the test results in $Z \leq 0{,}01$. If with $\varphi = 2\ K_g$ the test results in $Z \geq 1{,}0$, regime II is followed. Usually it is more convenient, given a known value of K_g and the inequalities for Z, to obtain the values of l_c and to estimate if such a value is realistic.[26] The results of the Z test are presented in Table III.

Assuming crystallization occurred in regime I, the crystals of the HDPE sample would have a thickness in the range between 0.2 and 1.5 Å, which is clearly unrealistic. Assuming that the crystallization occurs in regime II, the crystal thickness of the HDPE sample is in the range between 15 and 500 Å, which could be reasonable for HDPE. Regarding the PP and PA6 samples, an unrealistically high crystal thickness was obtained by assuming crystallization regime II. Therefore, it was assumed that the crystallization of the PP and PA6 sample belong to regime I or III. Accordingly, parameter ξ was assumed to be 4 for the PP and PA6, that is, 2 for the HDPE sample.

The relative size distribution of the critical nuclei was determined and presented in Figure 4. As can be seen, an increase of the cooling rate leads to a shift of the distribution curve in the direction of lower temperatures. This behavior is, as already discussed, the consequence of the reduced residence time with an increased cooling rate and is common for all three materials.

Table III. The Results of the Z Test

	l_c (Å)		
Substitution	PP + 0.5 wt % talc M10/M30	HDPE + 2 wt % talc M03	PA6 + 2 wt % bentonite
Regime I, III $Z = 0.01$; $\varphi = K_g$	35–295	0.2–1.5	3–58
Regime II $Z = 1.0$; $\varphi = 2\ K_g$	(2–127) × 10^4	15–500	(0.02–5.5) × 10^5

However, there is a large difference between the shape of the distribution curves of the PP and PA6 samples on the one hand [see Figure 4(a–c)] and the HDPE sample on the other [see Figure 4(d)]. The distribution curves, that is, the related peaks of the PP and PA6 samples become broader and smaller as they are shifted toward the lower temperatures. This shape change of the distribution curves is believed to be a consequence of the athermal effect, which stabilizes the subcritical nuclei. As opposed to PP and PA6, the distribution curves of the HDPE sample are simply transferred toward the lower temperatures, while more or less no change of the peak height is detected [see Figure 4(d)].

Furthermore, the peaks can be identified in Figure 4, which represents the thickness of the critical nuclei, most commonly found in distribution, which can be expected to be those with the fastest formation rate.

The Influence of the Filler Content at a Constant Cooling Rate

As shown, the cooling rate has an influence on the determined K_g due to the athermal and transient effects. However, after a certain cooling rate is achieved (~20 and 15 K/min for the PP and PA6, i.e. ~25 K/min for the HDPE samples) it seems that a further cooling rate increase leads to no further change of the nonisothermal effects. Consequently, K_g remains constant, as was shown in Figure 3. Additionally, the difference in the nucleation ability of two talc grades with different particle sizes seems to be visible only for the higher cooling rates. Therefore, the following part of this work was performed at a cooling rate of 30 K/min for the PP and HDPE, that is at 15 K/min for the PA6 samples.

In our previous contribution, the crystal structure of the same PP type filled with the talc of the same origin as used in this

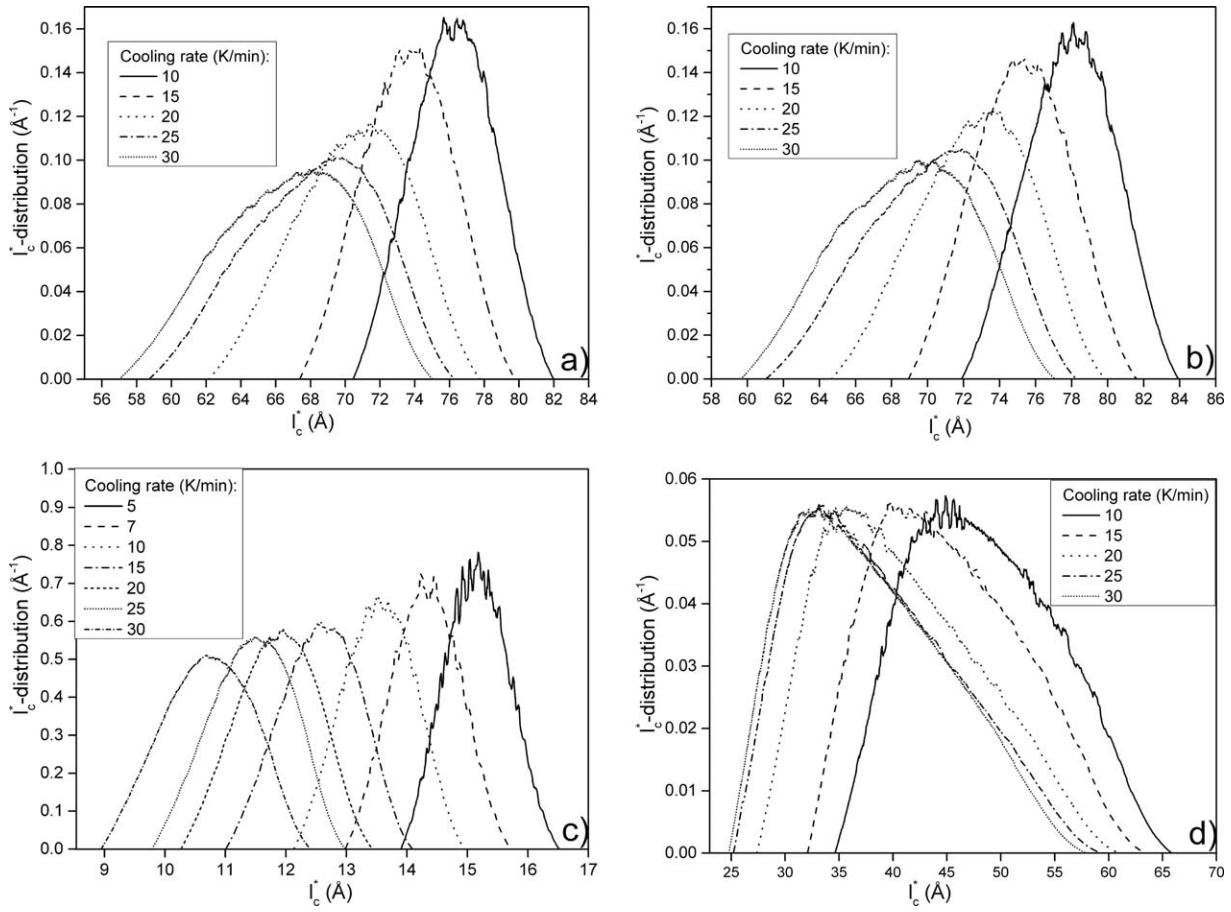

Figure 4. The relative size distribution of the critical nuclei during non-isothermal cooling at different rates for (a) PP with 0.5 wt % of Fintalc M10; (b) PP with 0.5 wt % of Fintalc M30; (c) PA6 with 2 wt % of bentonite; (d) HDPE with 2 wt % of Fintalc M03.

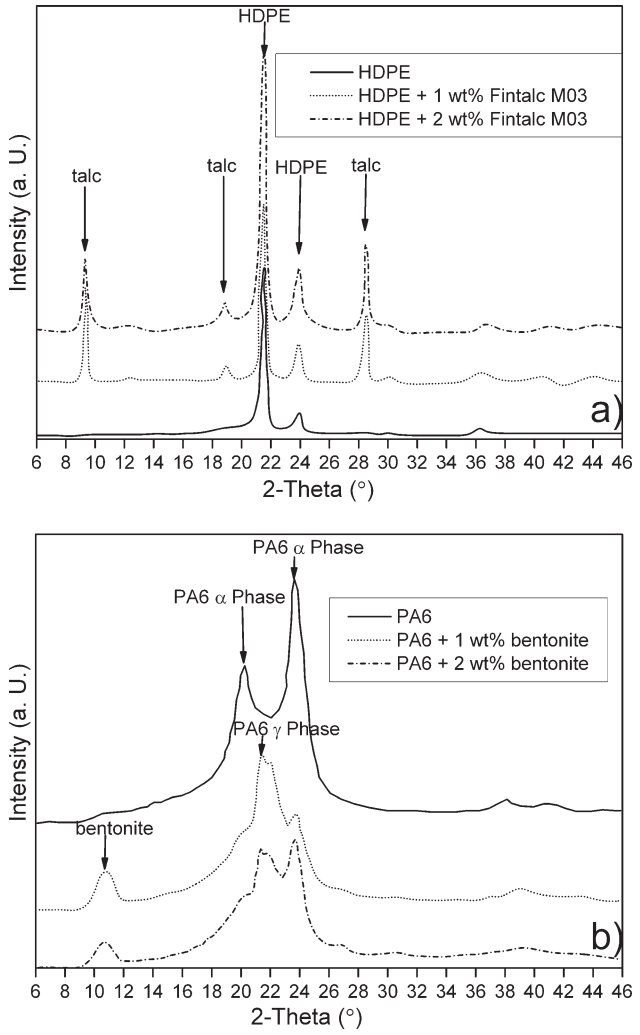

Figure 5. WAXS diffractograms of: (a) pure HDPE and HDPE with 1 and 2 wt % of Fintalc M03; (b) pure PA6 and PA6 with 1 and 2 wt % of bentonite.

work was determined with WAXS.[18] It was found that talc has no influence on the crystal structure of PP. Independently of the talc concentrations, only the α-form of i-PP was detected, with the characteristic peaks at $2\theta = 14$, 17 18.5, 21.5°. WAXS diffractograms of pure HDPE and of HDPE containing 1, and 2 wt % of Fintalc M03 as well as of pure PA6 and PA6 with 1 and 2 wt % of bentonite are presented in Figure 5. WAXS diffractograms of pure HDPE [see Figure 5(a)] show two maxima at $2\theta = 21.5°$ and 24.0°. These peaks come from 110 and 220 plane reflection of the orthorhombic unit cell of HDPE.[27] Upon the addition of 1 and 2 wt % of Fintalc M03, there is no change of the peak positions. This indicates that the pure HDPE and HDPE with 1 and 2 wt % of Fintalc M03 have the same crystalline structure. As can be seen in Figure 5(b), pure PA6 exhibits two intense reflections at $2\theta = 20.3°$ and 23.6°, which are characteristic of the monoclinic α crystalline form of PA6.[26,28] As indicated in the figure, the addition of bentonite leads to a disappearance of the PA6 peak at $2\theta = 20.3°$ and to a huge decrease of the peak at $2\theta = 23.6°$ as well as to a new peak at $2\theta = 21.3°$, which corresponds to the PA6 crystals in the γ phase.[29] This implies that upon the addition of bentonite PA6 crystallizes predominantly in γ-crystalline form. It has already been reported in literature that some layered nanoclays, for example, montmorillonite, can hinder the crystallization of PA6 by intercalating the PA6 molecular chains between the layers of nanoclay.[30] This reduces the mobility of the PA6 molecules and thus disables their orderly arrangement, which is necessary for crystallization in the thermodynamically more stable α-phase.

The DSC exotherms of the PP, HDPE, and PA6 samples with a varying content of the respective fillers are plotted in Figure 6. In Figure 6, the onset of crystallization (T_{onset}) is indicated. T_{onset} is the temperature in the non-isothermal DSC scan, at which the crystallization process starts. A shift of the crystallization onset temperature indicates a modification of the nucleation process.[31] As one can see in Figure 6(a), with increased talc content, there is a drastic increase of the crystallization onset temperature of PP from ~110°C for pure PP to ~118°C for PP with 1.5 wt % Fintalc M30 and 119.5°C for PP with 1.5 wt % Fintalc M10, respectively. As regards HDPE, only a slight increase of T_{onset} from ~118°C for pure HDPE up to ~120°C for HDPE with 3.0 wt % of Fintalc M03 occures [see Figure 6(b)]. The shift of the T_{onset} of PP and HDPE with an increased talc concentration occurs due to the nucleation ability of talc particles. The crystallographic structure of talc resembles that of the PP and HDPE. Therefore, the polymer crystals can be nucleated on the talc surface. As a consequence, the number of crystallization nuclei that is produced during simultaneous nucleation is increased. Such induced heterogeneous nuclei possess a lower fold surface free energy σ_e compared to that of the homogeneous nuclei, which are formed in the pure polymer melt. According to eqs. (2) and (6), the reduced fold surface free energy of the polymer nuclei leads to a decrease of the critical nuclei thickness l_σ^* that is of the nucleation parameter K_g. This corresponds to a decrease in the activation energy barrier for nucleation [see ΔGn^* in eq. (1)]. The decreased activation energy barrier can be easily overcome at a lower supercooling $T_m^0 - T$, that is, at a higher crystallization temperature. Thus, the crystallization of PP and HDPE starts at a higher T_{onset}, upon the introduction of talc. Furthermore, Fintalc M10 compared with Fintalc M30 possesses smaller particles, that is, a larger specific surface. This enables more area for the nucleation of PP crystals and is therefore responsible for the higher nucleation efficiency of Fintalc M10. This is reflected through the higher T_{onset} of the PP containing Fintalc M10. As opposed to PP and HDPE samples, the addition of bentonite reduces the T_{onset} of pure PA6 from ~185°C (pure PA6) up to ~182°C (PA6 with 3.0 wt % of bentonite), as shown in Figure 6(c). The bentonite particles present a physical obstacle for the movement of the PA6 chain segments in the molten state. As a consequence, the nucleation parameter K_g is expected to increase, leading to an increase in the activation energy barrier ΔGn^*. To achieve a higher energy barrier, a larger driving force for nucleation is needed, which corresponds to a higher super-cooling, that is, lower T_{onset}. Accordingly, T_{onset} of PA6 decreases upon the addition of bentonite, as can be seen in Figure 5(c).

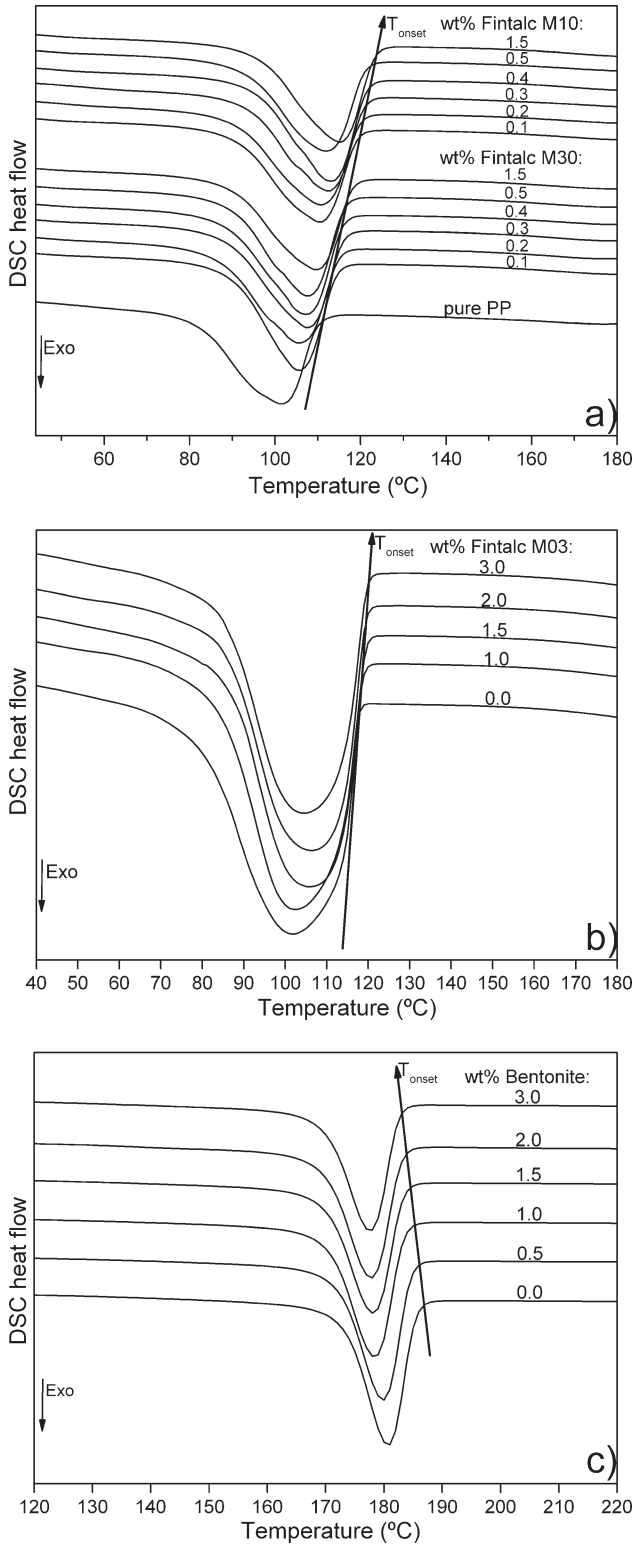

Figure 6. The influence of the filler content on the DSC exotherms of: (a) PP filled with Fintalc M10 and M30; (b) HDPE filled with Fintalc M03; (c) PA6 filled with Bentonite.

The observed change of the T_{onset} as a consequence of the nucleation or inhibition effect of the filler affects the further growth rate of the polymer crystals. For the higher crystallization temperature, the linear growth rate of the polymer crystals is lower and vice versa.[32] This should furthermore affect the final polymer morphology. In our previous work using the PP of the same type as well as the talc of the same origin, we showed that the increase in T_{onset} of PP from 118°C up to 128°C as a consequence of the nucleation activity of talc leads to an increase of crystal thickness and the degree of crystallinity of PP from 60 to 72 Å, that is, from 49 to 54%, respectively.[18] The characteristic SAXS patterns of the HDPE and PA6 samples as well as of pure bentonite are presented in Figure 7.

As can be seen in Figure 7(a–c), the SAXS patterns of pure HDPE and its composites show a high anisotropy. This anisotropy can be attributed to an extensive orientation of the HDPE molecules, which occurs in the flow direction during the film extrusion. In contrast, the SAXS patterns of PA6 presented in Figure 7(d–f) are essentially isotropic and are not indicative of any preferable orientation in the compression molded samples. From the Fourier transformation of the corresponding scattering functions, long period (D), crystal thickness (l_{SAXS}), and crystallinity (X_{SAXS}) as well as the interlayer distance of the bentonite clay particles or d-spacing (d) are obtained. Additionally, the degree of crystal orientation (ω) was calculated from the azimuthal scan of the SAXS patterns as the ratio between the base line intensity and the peak intensity. The SAXS results of the HDPE and PA6 samples are summarized in Table IV. As already expected on the basis of the DSC results and theoretical considerations, Fintalc M03 facilitates the nucleation of HDPE by lowering the surface free energy of HDPE critical nuclei. This enables the nucleation and subsequent growth of the HDPE crystals at a higher temperature, resulting in an increase of crystallinity from 56 up to 61% and of the crystal thickness from 83 up to 90 Å upon the addition of 2 wt % of Fintalc M03, respectively. By contrast, the addition of bentonite in PA6 inhibits the nucleation of PA6 and therefore leads to a decrease in crystallinity and crystal thickness from 35 to 22%, that is, from 35 to 22 Å, as shown in Table IV.

As shown, the obtained DSC and SAXS results confirm the nucleation activity of talc in the crystallization of PP and HDPE, that is, the inhibiting effect of bentonite in the crystallization of PA6. Accordingly, the mentioned effects should also be reflected through the change of the K_g value. The K_g of the PP, HDPE, and PA6 samples were determined using eq. (8) and as a function of the filler content presented in Figure 8. As shown in Figure 8(a), for pure PP the nucleation parameter K_g of 6,7 $\times$ 10^5 K^2 was obtained. This value agrees well with that of 7.28 $\times$ 10^5 K^2, obtained from the microscopic investigations of the isothermally crystallized PP.[33] The following decrease of K_g as the amount of talc is increased is a consequence of the nucleation activity of the talc. Fintalc M10 has smaller particles compared with Fintalc M30 and accordingly a larger specific surface area. This leads to more pronounced nucleation effects and therefore lower K_g values of PP filled with Fintalc M10, as indicated in Figure 8(a).

As shown in Figure 8(b), a K_g of 0.76 $\times$ 10^5 K^2 was obtained for pure HDPE. This value is slightly lower then 0.96 $\times$ 10^5 K^2, deduced from direct measurement of the spherulite growth rate by optical microscopy.[34] Furthermore, it can be seen that the K_g

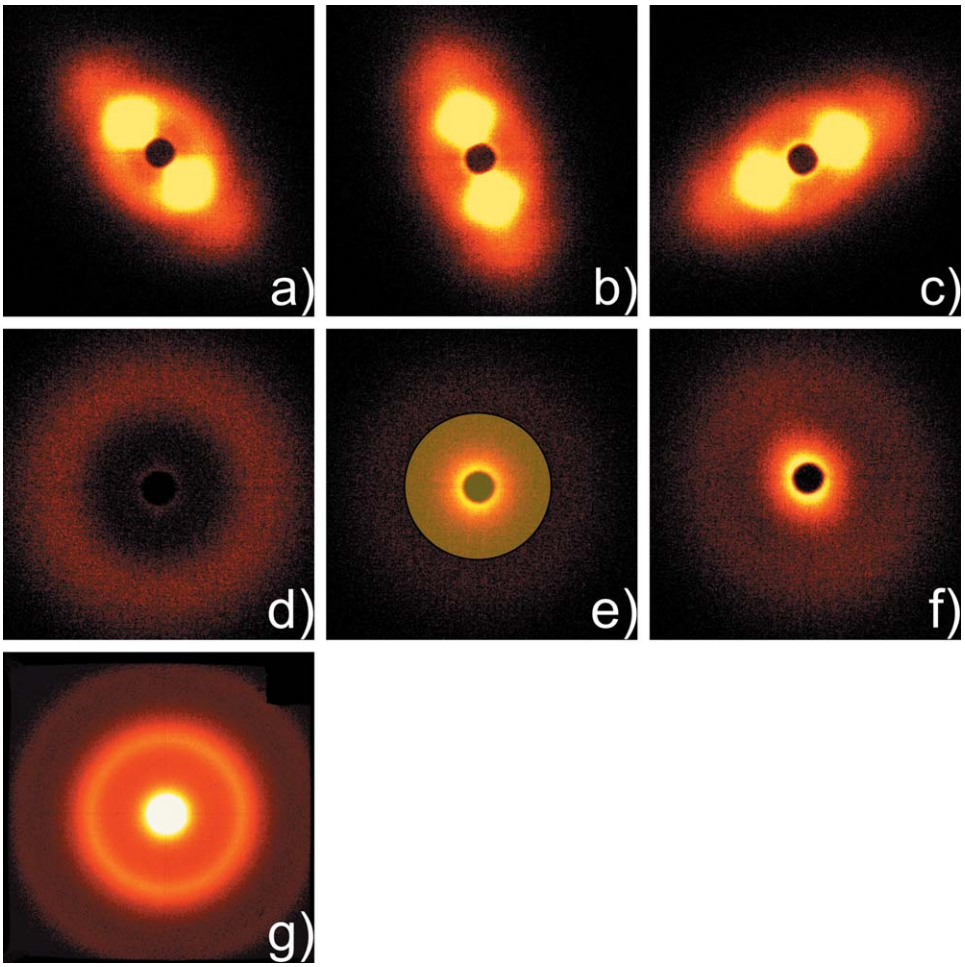

Figure 7. SAXS patterns of: (a) pure HDPE (b) HDPE with 1 wt % of Fintalc M03; (c) HDPE with 2 wt % of Fintalc M03; (d) pure PA6; (e) PA6 with 1 wt % of bentonite; (f) PA6 with 2 wt % of bentonite; (g) pure bentonite. [Color figure can be viewed in the online issue, which is available at wileyonlinelibrary.com.]

value of pure HDPE is noticeably lower compared to that of pure PP (6.7×10^5 K^2). Compared with PP, HDPE has small hydrogen atoms instead of methyl groups in its structure, enabling a zig-zag conformation of the HDPE chains. This enables the HDPE chains to be packed dense in the more stable orthorombic unit cells, compared with the monoclinic unit cells of PP.[4] As a consequence, HDPE possesses a higher heat of fusion of an ideal crystal ΔH_f^θ and therefore according to eq. (6) a lower K_g. Similarly to PP, talc has a nucleation effect for HDPE. Consequently, there is a clear tendency for the K_g of HDPE to decrease as the amount of talc is increased, as shown in Figure 8(c). Regarding pure PA6, a K_g value of 2.27×10^5 K^2 was obtained [see Figure 8(c)]. This value agrees well with the 2.33×10^5 K^2 obtained from nonisothermal crystallization of pure PA6 using the Vyazovkin model.[28] As a consequence of the inhibiting effect of bentonite on the nucleation of PA6, there is an increase of the K_g of PA6 upon the addition of bentonite, as shown in Figure 8(c).

In addition, by using the K_g values shown in Figure 8 and by applying the method presented in the previous section, the size distribution curves of critical nuclei were obtained. From the distribution curves, the most commonly found nuclei l^*_{peak} and related temperature T_{peak} were determined as peak values and used together with the crystal thickness measured with SAXS (l_c) to calculate the Hoffman-Weeks thickening coefficient

Table IV. The Long Period (D), Crystal Thickness (l_c), Crystallinity (X_{SAXS}), Orientation Degree (ω) as well as the Interlayer Distance of the Bentonite Clay Particles or d-Spacing (d) of the Samples Obtained from SAXS Measurements

Sample	D (Å)	l_c (Å)	X_{SAXS} (%)	ω (-)	d (Å)
HDPE	148	83	56	0.72	-
HDPE + 1 wt % talc	147	88	60	0.77	-
HDPE + 2 wt % talc	147	90	61	0.77	-
PA6	100	35	35	0.00	-
PA6 + 1 wt % bentonite	92	25	27	0.03	37
PA6 + 2 wt % bentonite	100	22	22	0.09	36
Bentonite	-	-	-	-	33

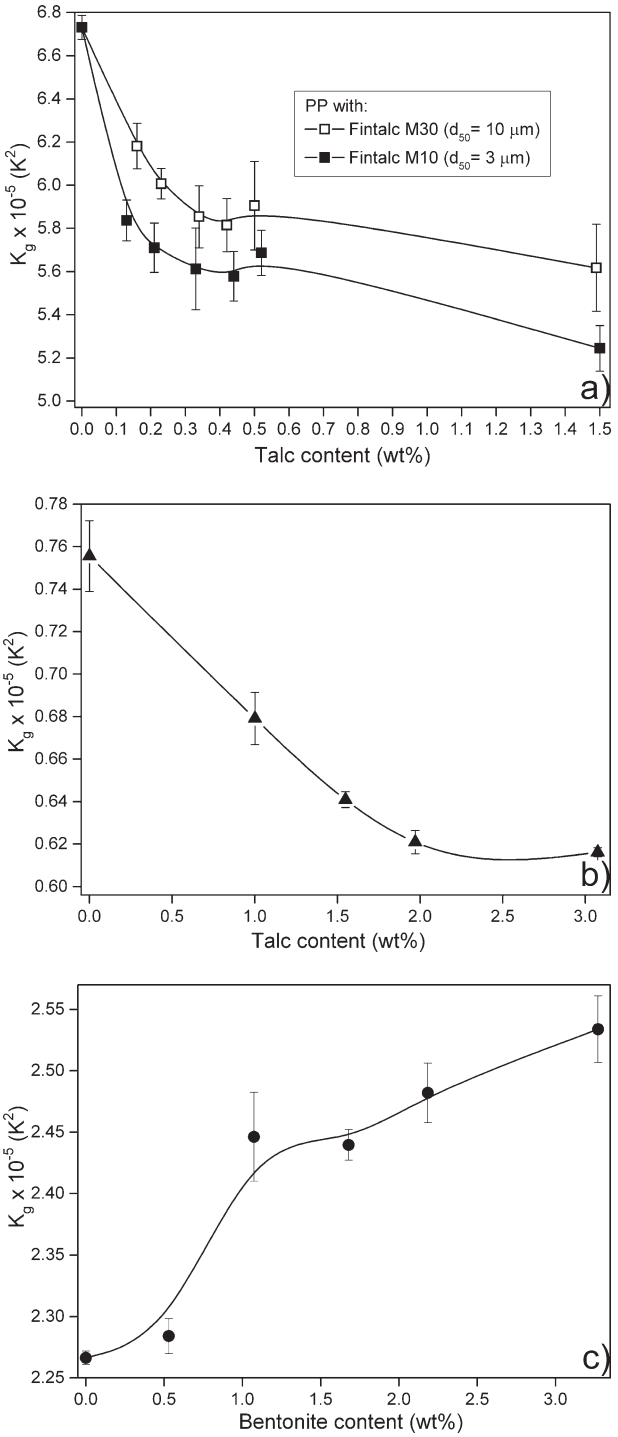

Figure 8. The influence of the filler content on the nucleation parameter K_g of: (a) PP filled with Fintalc M10 and M30; (b) HDPE filled with Fintalc M03; (c) PA6 filled with Bentonite.

(γ_{HW}) according to eqs (4) and (5). The results are shown in Table V.

A comparison of the final crystal thickness obtained under isothermal conditions with the initial crystal thickness calculated from kinetic theory gives values of γ_{HW} generally between 2 and 5, more precisely for polyethylene under normal conditions between ~2 and 2,5.[4] Therefore, γ_{HW} values obtained in this work agree well with those listed in literature, with the exception of PA6 with 1 and 2 wt % of bentonite, where somewhat lower values were obtained.

The Correlation of K_g with Young's Modulus and Yield Stress

According to the standard ISO 527, Young's modulus (E_y) is determined as a slope of the stress-strain curve, up to 0.25% of deformation. It is believed that such a low tensile deformation is primarily affected by the structure of amorphous regions between the crystals,[35] where several types of molecules can be distinguished. These are loops, which start and end in the same crystal, tails with one free end, floating molecules, which are unattached to any crystal as well as tie molecules, which join up two crystals.[36] Still, it is believed that the concentration and elastic properties of tie molecules are crucial for the stress transfer between the crystals and thus for the elastic properties of the material.[36,37] Thus, we assumed that only the amorphous phase, which consists of tie, loops, tails, and floating molecules, participates in the low strain deformation, such as that used for the determination of Young's modulus. Second, we divided the amorphous phase into two regions: the tie molecule region and the region with all the other molecule types. By using the simply mechanical model suggested by Takayanagi,[38] which implies the serial connection of two regions, the Young's modulus (E_y) of the material can be written in the following form:

$$\frac{1}{E_y} = \frac{1-\beta}{E_a} + \frac{\beta}{E_t} \tag{16}$$

where β is the volume fraction of the tie molecules, $1-\beta$ thus being the volume fraction of all the other molecules of the amorphous phase and E_t and E_a are the elastic modulus of the tie molecules and amorphous phase, respectively. The number of tie molecules and therefore its volume fraction β is expected to be greater with the increasing of the number of nuclei.[39] As shown, talc acts as a nucleation agent by decreasing the surface free energy (i.e., nucleation parameter K_g) of PP, which has as consequence the increased number of PP nuclei. Thus, the lower the K_g, the higher the nuclei concentration and consequently the higher the volume fraction of the tie molecules (β), which finally leads to an increase in E_y. Let us now assume that there is some mathematical linkage, which connects K_g and β. Let it be for the first approximation a simple function of the $\beta = y/K_g$

Table V. The Thickness of the most Commonly Found Nuclei (l^*_{peak}), Thickness Increment (δl), Crystal Thickness (l_c) and Hoffman-Weeks Thickening Coefficient (γ_{HW}) for Pure HDPE and HDPE with 1 and 2 wt % of Fintalc M03 as well as for Pure PA6 and PA6 with 1 and 2 wt % of Bentonite

Sample	l^*_{peak} (Å)	δl (Å)	l_c (Å)	γ_{HW} (-)
HDPE	38.2	4.9	83	1.9
HDPE + 1 wt % talc	34.2	4.9	88	2.3
HDPE + 2 wt % talc	32.6	4.9	90	2.4
PA6	12.0	1.5	35	2.6
PA6 + 1 wt % bentonite	12.4	1.4	25	1.8
PA6 + 2 wt % bentonite	12.6	1.4	22	1.6

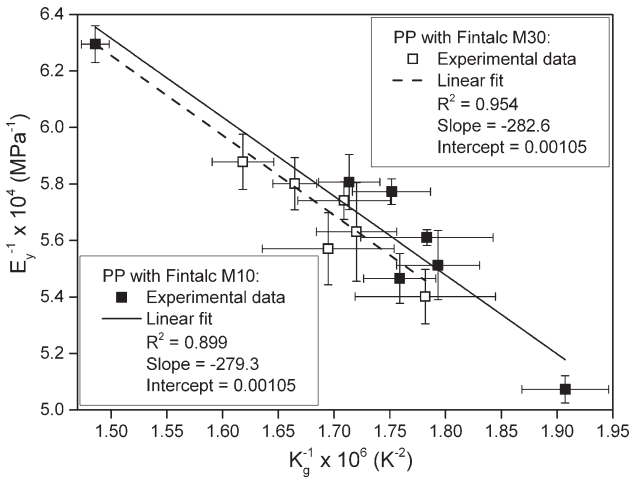

Figure 9. The correlation of the experimentally determined reciprocal of Young's modulus (E_a^{-1}) with the reciprocal of the nucleation parameter (K_g^{-1}) for PP filled with Fintalc M10 and M30.

type, where y may be considered as a constant. Therefore, by assuming that $E_t >> E_a$, eq. (16) can be written in the form:

$$\frac{1}{E_y} = \frac{1}{E_a} - \frac{y}{E_a}\frac{1}{K_g} \tag{17}$$

The correlation of the experimentally determined E_a^{-1} with K_g^{-1} for PP filled with Fintalc M10 and M30 is presented in Figure 9. As can be seen, the experimentally obtained values of E_y^{-1} and K_g^{-1} fit well with eq. (17). A somewhat better correlation was, however, obtained for PP filled with Fintalc M30 (correlation coefficient $R^2 = 0.954$) compared with PP filled with Fintalc M10 ($R^2 = 0.899$). The negative slopes of the linear correlations obtained indicate an increase in E_y with a decrease in K_g. This trend agreed well with the trend assumed. The intercepts of the linear correlations presented in Figure 9 correspond to the value of E_y, where $K_g^{-1} = 0$, that is, where K_g tends to infinity. The infinity value of K_g means, in other words, the infinity of the activation energy barrier of crystallization. Under this circumstance the sample would be 100% amorphous and thus would have a Young's modulus (E_y) equal to that of the amorphous phase (E_a). Therefore, E_a can be determined from the intercept of the linear correlations shown in Figure 9. For both samples, the same intercept value is obtained and amounts to 0.00105 MPa^{-1}. The reciprocal of the obtained intercept corresponds according to eq. (17) to the Young's modulus of the amorphous phase of PP and amounts to 952.4 MPa.

Contrary to Young's modulus, the yield stress of the semicrystalline polymers above their glass transition temperature is determined by the yield stress required for crystal deformation and not by the amorphous phase.[35] The thinner and more imperfect the crystals, the lower the stress required for their deformation. Thus, there is a strong dependence between the crystal thickness of the semicrystalline polymers and the yield stress. O'kane and co-workers have shown that the crystal thickness of PP films determined via SAXS (l_c) correlate linearly with the yield stress of the samples (σ_y).[40] Since l_c depends on the nucleation parameter (K_g) through eqs. (2), (3), (5), and (6), it can be expected that there is some direct dependence between σ_y and K_g. This dependence is shown in Figure 10 for PP with Fintalc M10 and M30. As can be seen, the experimental data fall on a straight line with the intercepts of 47.1 and 48.5 MPa, respectively. Accordingly, the samples exhibit a finite yield stress at zero K_g. The zero K_g value corresponds to zero activation energy to crystallization. In such a case, the sample would be 100% crystalline, having all macromolecules fully stretched and ideally attached in the crystal. Such ideal crystals would have a maximal thickness, which corresponds to the length of the macromolecular chains. According to the dislocation theory, the deformation of polymer crystals at yield point is considered in terms of the dislocation motion within the crystals.[41] Accordingly, the dislocations will form most easily within the thinnest crystals, a result, which has been confirmed by the microscopy study.[42] Thus, the polymer with zero K_g and therefore with the perfect crystals of a maximal thickness would have an ideal yield stress.

Following Kelly, the theoretical yield stress (σ_{max}) when there is no thermal activation of dislocations is given by[43]:

$$\sigma_{max} = \frac{Gr}{2\pi h} \tag{18}$$

where G is the shear modulus of polymer crystals, which have been reported to be in the range 0,84–1,00 GPa for PP,[40] r is the Burger's vector of the dislocation formed by deformation within the crystalline regions, which is assumed to be equivalent to the c axis of the PP monoclinic unit cell[44] and h is the separation of the planes in the crystal unit, where the dislocation occurs. Assuming that the dislocations occur in the 010 plane of PP, h is equivalent to the b axis of the PP monoclinic unit cell.[40] In our previous contribution, it was shown that talc has no influence on the unit cells of the PP crystals. Irrespective of the talc amount, only the monoclinic unit cells with the c and b dimensions of 6.50 and 21.07 Å have been found.[18] Using these values together with the G of 0.92 GPa, which was calculated as the arithmetic mean of the values reported in literature, the theoretical yield stress σ_{max} of 45.2 MPa is obtained. This value is comparable with the values of 47.1 and 48.5 MPa, obtained as the corresponding intercepts at zero K_g in Figure 10.

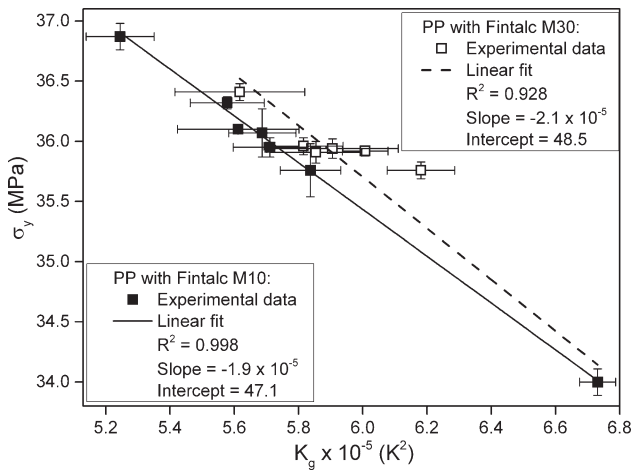

Figure 10. The dependence of yield stress (σ_e) upon the nucleation parameter (K_g) of PP with Fintalc M10 and M30.

In contrast to PP, the obtained K_g values of the HDPE and PA6 materials show no plausible correlation with the modulus and yield stress (data not shown). Regarding HDPE, the possible reason for the absence of correlations could be the orientation of the HDPE molecules [see Figure 7(a–c) and Table IV], which can leads to an increase of Young's modulus and yield stress of ~20- and 5-fold, respectively.[2] We believe that this effect had a much greater influence on the elastic modulus and yield stress of HDPE samples, compared with morphology changes, which occur as a consequence of the nucleation effect of talc. When speaking about the PA6 samples, the strong reinforcing effects of a nano-filler such as bentonite could be responsible for the absence of a correlation between mechanical properties and K_g. In contrast to talc, where the particles are in the order of microns, the single layers of bentonite are ~1 nm thick, with the other two dimensions much more pronounced than the thickness. Accordingly, bentonite possesses a high aspect ratio. Therefore, if properly separated and dispersed, nano fillers such as bentonite with only 1 wt % of loading lead to a nearly 8-fold increase in Young's modulus.[45] In this work, the increase of the d-spacing of bentonite added in PA6 compared with that of pure bentonite was confirmed with SAXS (see Table IV). This is a consequence of the intercalation of the PA6 molecules into the galleries between the bentonite layers. Thus, some micromechanical (reinforcement) effects of bentonite in the PA6 matrix are highly probable. This micromechanical effect could be dominant over the morphological effect, thus leading to an absence of the expected correlations with K_g.

SUMMARY AND CONCLUSIONS

This approach provides an opportunity to apply a single DSC scan to determine the nucleation parameter (K_g) as well as the size distribution of the critical nuclei, from which the most commonly found fraction (l^*_{peak}) can be obtained as the peak value. The parameters obtained in this way from the calorimetric experiments are related to the Young's modulus and yield stress of the samples. Several conclusions may be proposed:

- Due to the nonisothermal effects, the DSC cooling rate up to a certain value has an influence on the determined K_g. Afterwards, K_g reaches a plateau and shows no further changes with the cooling rate.
- There is a good agreement between the K_g values obtained in this research and those found in literature as regards pure PP, HDPE, and PA6.
- Talc has a positive nucleation effect on the crystallization of PP and HDPE. This leads to decreased K_g and l^*_{peak} with an increased talc content. An opposite trend was found upon the addition of bentonite in PA6, where bentonite had an inhibitory effect on the crystallization of PA6.
- As confirmed, the obtained parameters are related to the sample morphology and thus to the mechanical behavior of semicrystalline polymers. Accordingly, it was shown that the obtained K_g correlates well with the Young modulus and yield stress as regards PP samples. For this, simply linear models were proposed. Therefore, the proposed methods could be one new way to establish the mathematical correlations between thermoanalytical methods (DSC measurements), morphology, and the mechanical behavior of polymer materials.

ACKNOWLEDGMENTS

Helpful discussions with P. Löbmann and G. Sextl are gratefully acknowledged. The authors thank T. Delic for performing the language correction.

APPENDIX

Table AI. The Crystallographic, Thermodynamic, and Nucleation Constants Used in This Study

Quantity	PP[10,46]	HDPE[47]	PA6[48]
Crystallographic			
a_0, Width of the chain stem (nm)	0.670	0.742	0.956
b_0, Thickness of the chain stem (nm)	0.656	0.490	0.801
Thermodynamic			
ΔH_f^0, heat of fusion of an ideal crystal	134[a]	280[a]	232[a]
	206[b]	293[b]	230[b]
T_m^0, equilibrium melting temperature (K)	481	418	502
T_∞, temperature at which there is no chain motion (K)	223	233	293
Nucleation constants			
$\sigma \times 10^{-3}$, side surface free energy (J/m^2)	8.79	11.80	33.00
U, activation energy for the transport of polymer segments (J/mol)	6280	6280	6222

[a] $\times 10^6$ J/m^3.
[b] J/g.

REFERENCES

1. Muthukumar, M. *Adv. Chem. Phys.* **2004**, *128*, 1.
2. Ehrenstein, G. W. Polymeric Materials; Carl Hanser Verlag: München, **2001**.
3. Kurz, W.; Fisher, D. J. Fundamentals of Solidification; Trans Tech Publications: Aedermannsdorf, **1984**.
4. Basset, D. C. Principles of Polymer Morphology; University Press: Cambrige, **1981**.
5. Martins, A. J.; Pinto, J. J. C. C. *Polymer* **2002**, *43*, 3999.
6. Marand, H.; Xu, J.; Srinivas, S. *Macromolecules* **1998**, 31.
7. Hoffmann, J. D.; Weeks, J. J. *J. Res. Natl. Bur. Stand.* **1962**; *A66*:13.
8. Papageorgiou, G. Z.; Achilias, D. S.; Bikiaris, D. N.; Karayannidis, G. P. *Thermochim. Acta* **2005**, *427*, 117.

9. Hoffmann, J. D.; Davis, G. T.; Lauritzen, J. L. Tratise on Solid State Chemistry; Plenum Press: New York, **1976**; Vol. 3.
10. Feng, Y.; Jin, X.; Hay, N. *J. Appl. Polym. Sci.* **1998**, *69*, 2089.
11. Phillips, J. P. *Rep. Prog. Phys.* **1990**, *53*, 549.
12. Hoffman, J. D.; Ross, G. S.; Frolen, L.; Lauritzen, J. I. *Res. Natl. Bur. Stand.* **1975**, *79A*, 671.
13. Kishore, K.; Vasanthakumari, R. *Colloid Polym. Sci.* **1998**, *266*, 999.
14. Lim, G. B. A.; McGuire, K. S.; Lloyd, D. R. *Polym. Eng. Sci.* **1993**, *33*, 537.
15. Vyazovkin, S.; Sbirrazzuoli, N. *Macromol. Rapid. Commun.* **2004**, *25*, 733.
16. Vyazovkin, S.; Dranca, I. *Macromol. Chem. Phys.* **2006**, *207*, 20.
17. Monasse, B.; Haudin, J. M. *Colloid. Polym. Sci.* **1986**, *264*, 117.
18. Kocic, N.; Kretschmer, K.; Bastian, M.; Heidemeyer, P. *J. Appl. Polym. Sci.* **2012**, *126*, 1207.
19. Yiping, P.; Guangmei, C.; Zhen, Y.; Hongwu, L.; Yong, W. *Eur. Polym. J.* **2005**, *41*, 2753.
20. Alberola, N.; Cavaille, J. Y.; Perez, J. *J. Polym. Sci.* **1990**, *28*, 569.
21. Long, Y.; Shanks, R. A.; Stachurski, Z. H. *Prog. Polym. Sci.* **1995**, *20*, 651.
22. Sajkiewicz, P. *J. Polym. Sci. Part B: Polym. Phys.* **2002**, *40*, 1835.
23. Sajkiewicz, P. *J. Polym. Sci. Part B: Polym. Phys.* **2003**, *41*, 68.
24. Ziabicki, A.; Sajkiewicz, P. *Colloid. Polym. Sci.* **1998**, *276*, 680.
25. Lauritzen, J. I. *J. Appl. Phys.* **1973**, *44*, 4353.
26. Wu, T. M.; Lien, Y. H.; Hsu, S. F. *J. Appl. Polym. Sci.* **2004**, *94*, 2196.
27. Gupta, A. K.; Rana, S. K.; Deopura, P. L. *J. Appl. Polym. Sci.* **1992**, *44*, 719.
28. Guo, B.; Zou, Q.; Lei, Y.; Du, M.; Liu, M.; Jia, D. *Thermochim. Acta* **2009**, *484*, 48.
29. Campou, I.; Gomez, M. A.; Macro, C. *Polymer* **1998**, *39*, 6279.
30. Tjong, S. C.; Bao, S. P. *J. Polym. Sci. Part B: Polym. Phys.* **2004**, *42*, 2878.
31. Ou, C. F. *Eur. Polym. J.* **2002**, *38*, 467.
32. Cebe, P. *Polym. Compos.* **1988**, *9*, 271.
33. Monasse, B. Doct. Ing. Thesis, Ecole Nationale Superieure des Mines de Paris, Paris, 1982.
34. Hoffman, J. D.; Miller, R. D. *Polymer* **1997**, *38*, 3151.
35. Karger, J. K. Nano- and Micro-mechanics of Polymer Blends and Composites; Carl Hanser Verlag: München, **2009**.
36. Spitalsky, Z.; Bleha, T. *Polymer* **2003**, *44*, 1603.
37. Janimak, J. J.; Stevens, G. C. *J. Mater. Sci.* **2001**, *36*, 1879.
38. Takayanagi, M.; Imada, K.; Kajiyama, T. *J. Polym. Sci. C* **1966**, *15*, 263.
39. Brown, N. *J. Mater. Sci.* **1983**, *18*, 1405.
40. O'kane, W. J.; Young, R. J.; Ryan, A. J. *J. Macromol. Sci. B* **1995**, *34*, 427.
41. Young, R. J. *Philos. Mag.* **1974**, *30*, 85.
42. Olley, R. H.; Basset, D. C. *J. Macromol. Sci. Phys.* **1994**, *B33*, 211.
43. Kelly, A. A Strong Solids; Clarendon Press: Oxford, **1966**.
44. Quirk, R. P.; Asamarraie, M. A. Polymer Handbook; Wiley Interscience: New York, **1989**.
45. Utracki, L. A. Clay-Containing Polymeric Nanocomposites; Rapra Technology Limited: Shropshire, **2004**.
46. Menczel, J.; Varga, J. *J. Therm. Anal.* **1983**, *28*, 161.
47. Xu, J. T.; Zhao, Y. Q.; Wang, Q.; Fan, Z. Q. *Macromol. Rapid Commun.* **2005**, *26*, 620.
48. Huang, J. W.; Chang, C. C.; Kang, C. C.; Yeh, M. Y. *Thermochim. Acta* **2008**, *468*, 66.